ISSN 0036-0295, Russian Metallurgy (Metally), Vol. 2021, No. 7, pp. 842–855. © Pleiades Publishing, Ltd., 2021.
Russian Text © The Author(s), 2021, published in Metally, 2021, No. 4, pp. 41–55.

# Changes in the Structural-Phase State and Mechanical Properties of $Ni_3Al$–Ni–NiAl Cast Alloys Containing Chromium, Molybdenum, Tungsten, Rhenium, and Cobalt after Heat Treatment

**K. B. Povarova[a, *], A. A. Drozdov[a, b], O. A. Bazyleva[c], A. E. Morozov[a], A. V. Antonova[a], M. A. Bulakhtina[a], and N. A. Alad'ev[a]**

[a] *Baikov Institute of Metallurgy and Materials Science, Russian Academy of Sciences, Moscow, Russia*
[b] *Bardin Central Research Institute of Iron and Steel Industry, Moscow, Russia*
[c] *FGUP GNTs RF VIAM, Moscow, Russia*
**e-mail: povarova@imet.ac.ru*

Received February 11, 2021; revised March 23, 2021; accepted March 31, 2021

**Abstract**—The influence of the temperature–time parameters (temperature from 1000 to 1300°C, time from 1 to 500 h) of heat treatment (HT) of ⟨001⟩ and ⟨111⟩ single crystals of boron-free heterophase γ′-$Ni_3Al$ + γ-Ni intermetallic (IM) alloys of the Ni–Al–Cr–Mo–W–Ti(Zr)–La system (VKNA-1V) and such alloys with cobalt and rhenium (VKNA-25) on their structure, fracture, and short-term and long-term strength is studied. The introduction of cobalt and rhenium or an increase in the cooling rate of the ⟨001⟩ single crystals in the range 30–300°C/min is found to decrease the sizes of the structural components of all levels. In addition, the rule derived for two- and three-component nickel-based alloys is shown to be valid for γ′-$Ni_3Al$-based IM alloys: if an introduced alloying element (AE) increases the melting point $T_m$ of the base metal (nickel), the AE distribution coefficient is $k_d > 1$ and the AE enriches dendrite arms; if AE decreases $T_m$ of nickel, we have $k_d < 1$ and the AE enriches the interdendritic space. The AE dendritic microsegregation coefficients $k_d$ weakly depend on the cooling rate during solidification, and their values decrease in the following row: Re, W, Co, Mo, Al, and Ti. An increase in the time of low-temperature HT ($T < T_{solvus}$) or an increase in the HT temperature to $T_{solvus} \le T \le T_{solidus}$ leads to the "homogenization" of heterophase γ′ + γ IM alloys. The dendritic microsegregation coefficients of all AEs except for Re approach unity, and interdendritic nonequilibrium $\gamma'_{pr}$ and γ′ + β precipitates disappear. A homogeneous γ′ + γ structure, which is characteristic of IM dendrites (γ′-phase regions of irregular shape separated by continuous or discontinuous γ-phase layers), forms. It differs from the structure of nickel superalloys. This type of homogenization decreases the durability as compared to the as-cast material, which retains the maximum microsegregation heterogeneity after short-term HT in order to relieve casting stresses.

**Keywords:** nickel aluminide, intermetallic compound, single crystal, heat treatment, microsegregation, structure, heat resistance, durability

**DOI:** 10.1134/S0036029521070090

## INTRODUCTION

Active works on creating heterophase γ + γ′ nickel superalloys (NSAs) as the main material for aircraft engine construction worldwide began in the middle of the last century. During this time, complex alloying systems were perfected; fundamentally new processes for manufacturing products, including those with a directional and single-crystal structure for critical parts of the hot gas path of gas turbine engines (GTEs), were developed; and the thermomechanical processing conditions that ensure the formation of optimal structural and phase states in products, which are responsible for the high-temperature characteristics of alloys, were determined [1–5]. The operating temperatures $T_{op}$ of cast γ + γ′ NSAs were increased from 950–980°C in the 1950s to 1100–1150°C in the 2000s–2010s due to intense alloying with refractory and rare metals (total content of heavy refractory alloying elements (AEs) was Σ = (W + Mo + Nb + Ta + Re) > 20 wt %, and the density increased to ~9 g/cm$^3$) and to the optimization of production processes and heat-treatment (HT) conditions.

A further increase in the operating temperatures of these materials for GTEs is associated with the development and use of alloys based on nickel aluminide γ′-$Ni_3Al$, which can operate at 1100–1200°C for a long time at temperatures and and at 1250–1300°C for a short time [6–9].

$Ni_3Al$-based alloys are lighter than second- and third-generation NSAs (for example, ZhS36, PWA-1484, CMSX-10, RENE-5, RENE-6, etc.) due to a higher aluminum content and a lower (by 1.5–2.3 times) content of heavy refractory metals [1, 5, 10, 11].

Interest in the alloys based on the γ'-$Ni_3Al$ intermetallic compound with and without boron microadditives has intensified since the 1980s [12–20]. Naturally, the scale and intensity of research aimed at studying and optimizing the alloying systems of this nickel aluminide and at developing technological processes for their production and methods for forming rational (or optimal) structural-phase states in them are disproportionately less than they were and still are involved in the creation of modern NSAs. This did not prevent us from achieving some success in the development of intermetallic (IM) alloys.

The heat-resistance characteristics of cast γ'-$Ni_3Al$ + γ-Ni are determined primarily by the fact that their heterophase structure with coherent or semicoherent joining of γ' and γ phases with an ordered ($L1_2$) and disordered fcc crystal lattice, respectively, is preserved up to solidus temperature $T_{solidus}$, in contrast to NSAs, in which a single-phase γ field exists at $T_{solvus} \le T \le T_{solidus}$, $(\gamma + \gamma') \rightarrow \gamma \rightarrow (\gamma + L)$. As a result, NSAs soften because of the dissolution of the strengthening γ'-$Ni_3Al$ phase [21].

The basic system of alloying γ'-$Ni_3Al$-based IM alloys was formed in the last decade of the 20th century (composition in wt %): Ni–Al(~8–9)–Cr(~7–8)–Mo(1.5–3)–Zr(0.6–1.6)–B(0.02–0.1). An example is the well-known alloys intended for use in both single-crystal and deformable versions: IC221M (Oak Ridge National Lab), IC396M and IC438 (Lockheed Martin Energy Research Corp.), and so on. Ni–Al–Mo–B alloys (without chromium, but with an increased (up to 14 wt %) molybdenum content) of the IC6 and IC6SX types, the properties of which are being tried to improve by the introduction of rhenium and yttrium, are being developed [22–24]. The company Textron Inc. also offers chromium-free $W_2B$-hardened γ'-$Ni_3Al$ + β-NiAl) alloys of the ISC8 type containing (wt %) 10–13 Al, 5–10 Ti, 6.8 Mo, 6.8 W, and 0.1 B. Alloys of the IC10 type with an increased (12.4 wt %) content cobalt were studied in [25–27]. Attempts are being made to create alloys with new alloying systems, e.g., an alloy containing 13.7 wt % Mo and 11.7 wt % Fe [28, 29]. It should be noted that all IM alloys of the IC type mentioned above contain boron as an AE, which provides low-temperature ductility of the metal. The disadvantage of $Ni_3Al$-based alloys with boron is the probability of a decrease in the melting point due to the formation of boron-containing eutectic and a high susceptibility to hot-shortness (decrease in the ductility at 300–850°C in air due to the penetration of oxygen into boron-enriched grain boundaries).

A separate group is represented by boron-free IM alloys of the types VKNA-1V (Ni–Al–Ti–Cr–Mo–W system) and VKNA-4U and VKNA-25 (the same system, additional alloying with Co and Re), the development of which was started at the end of the twentieth century (FGUP VIAM, IMET RAS). They demonstrate high heat-resistance characteristics in combination with a good low-temperature ductility, which is achieved due to the presence of a ductile structural component, namely, 10–15 vol % γ-Ni (nickel-based solid solution), in the structure of the alloys [18, 30–32].

The structural-phase state and, consequently, the mechanical properties of cast IM alloys produced by directional solidification (DS) undeformable alloys strongly depend on the solidification parameters, such as temperature gradient $G$, solidification rate $R$, and cooling rate during solidification $GR$ [22, 30, 31, 33–35], and on the temperature–time HT parameters of cast products [32, 36].

One of the important factors that determine the structure and properties of the single crystals of cast nickel and $Ni_3Al$-based IM undeformable alloys is dendritic microsegregation, i.e., a nonuniform AE distribution over the cross section of a dendritic cell at a uniform element distribution over the height and cross section of a single crystal. The problem of eliminating dendritic microsegregation in NSAs is solved by multistage HT, which includes long-term homogenization in the single-phase region of γ solid solutions located between the heterophase $\gamma + \gamma'_{sec}$ field and the $T_{solidus}$ line and subsequent alternation of dissolution–aging cycles. This treatment makes it possible to form homogeneous $\gamma + \gamma'_{sec}$ structures with specified morphology and particle sizes of the hardening $\gamma_{sec}$ phase of various genesis and the optimum γ/γ' misfit, which are responsible for the high heat-resistance characteristics of NSAs.

For cast γ'-$Ni_3Al$ + γ-Ni IM alloys of the VKNA type, this type of homogenization is impossible to eliminate dendritic microsegregation, since they retain a complex heterophase structure until the beginning of melting ($T_{solidus}$). Therefore, the question arises: To what extent is the homogenization of cast γ'-$Ni_3Al$ + γ-Ni IM alloys necessary to improve their heat-resistance characteristics? The results of a few scattered studies of the effect of long- and short-term heating of single-crystal cast alloys during HT (high-temperature annealing aimed at reducing microsegregation and low-temperature annealing–aging aimed at the precipitation of $\gamma'_{sec}$ particles of different levels of dispersion) on their structure and heat resistance do not allow us to answer this question unambiguously [36, 37]. In addition, these studies were carried out on alloys with a different character of microalloying.

The present study was carried out on boron-free high-temperature cast γ' + γ alloys of the Ni–Al–Cr–

**Table 1.** Content (wt %) of the main AEs* in alloys VKNA-1V (numerator) and VKNA-25 (denominator)

| Al | Ti | Cr | Co | Mo | W | Re | W + Re + Mo |
|---|---|---|---|---|---|---|---|
| 8.60 / 8.37 | 1.60 / 0.52 | 5.7 / 5.7 | – / 4.5 | 3.10 / 5.14 | 3.5 / 3.0 | – / 1.6 | 6.60 / 9.74 |

* REM was added to the IM alloy charge, namely, 0.015 wt % in the VKNA-1V alloy and 0.2 wt % in the VKNA-25 alloy.

Mo–W–Ti(Zr, Hf)–La(REM) alloying system (VKNA-1V, alloy of the first type) and the same system but with rhenium and cobalt (VKNA-25, alloy of the second type). An analysis of the structure of the ternary phase diagrams of these systems showed that there are fundamental differences in the solidification schemes in the vicinity of the γ′-$Ni_3Al$ and β-NiAl phases and in the characters of influence of the main AEs at their concentrations up to 10 at % on the phase composition and structure of multicomponent alloys VKNA-1V, VKNA-25, and VKNA-4U [21]. In the alloys of the second type (VKNA-4U, VKNA-25 with cobalt at the same aluminum content), the following two-phase interdendritic precipitates form: inside the γ′-$Ni_3Al$ phase, β-NiAl precipitates in the form of a degenerate eutectic $L \rightleftarrows \gamma' + \beta$ form. In the alloys of the first type (VKNA-1V, without cobalt), there are no β-NiAl precipitates.

When heated during HT or at the operating temperatures, the alloys undergo simultaneous processes associated with weakening or elimination of dendritic microsegregation and structural-phase transformations, resulting in the disappearance of primary $\gamma'_{pr}$ phase precipitations and nonequilibrium $\gamma'_{pr} + \beta$ phase precipitates and in the precipitation or dissolution of secondary $\gamma'_{sec}$ particles [21].

The purpose of this work is to study the effect of short- and long-term HT in the temperature range 1000–1300°C on the structure and mechanical properties of cast alloys of the first (VKNA-1V) and second (VKNA-25) types.

## EXPERIMENTAL

We studied VKNA-1V and VKNA-25 alloys, the chemical compositions of which are given in Table 1.

Single crystals of the alloys with ⟨111⟩ and ⟨001⟩ crystallographic orientations (COs) were prepared by DS, cooling rate *GR* was varied within 60–150 and 30–300°C/min ranges for the VKNA-1V and VKNA-25 alloys, respectively, the deviation from a specified CO direction did not exceed 10°, and the misorientation between structure blocks was ≤2°. HT of the alloys was carried out in SNOL furnaces in an air atmosphere, and cooling was performed in air. The microstructures of the alloys were studied by optical microscopy (OM), scanning electron microscopy (SEM), and transmission electron microscopy (TEM) on an Olympus GX-51 microscope and a LEO 1420 microscope equipped with an INCA Energy 300 energy-dispersive microanalyzer (Oxford Instruments and Tecnai G2 F20 S-TWIN). Electron-probe microanalysis (EPMA) was performed in the transmission scanning electron microscopy (TSEM) mode to detect high-angle scattered electrons and in the SEM mode. Long-term high-temperature durability tests were carried out on computerized ZST2/3-VIET stands using cylindrical samples with a gage portion diameter and length of 5 and 25 mm, respectively.

## RESULTS AND DISCUSSION

### *Cast Alloys: Microstructure and Microsegregation*

The effect of DS conditions on the structural component size in as-cast samples was studied on ⟨001⟩ single crystals of the alloys of the first and second types. Regardless of the cooling rate during solidification, all alloys have a dendritic–cellular structure represented by two-phase γ′-$Ni_3A$ + γ-Ni dendrites and coarse primary γ′-$Ni_3Al_{pr}$ precipitates in the interdendritic space (Fig. 1). In dendrites, γ′-$Ni_3Al$ regions are separated by thin (sometimes discontinuous) layers of the nickel-based γ solid solution.

Using transverse polished sections we determined the following parameters: the dendrite arm spacing, the sizes of the primary γ′-phase particles $\gamma'_{pr}$, or degenerate γ′ + γ eutectic) formed during solidification in the interdendritic space, the sizes of the γ′-phase regions in dendrites between γ-phase layers both in the interdendritic space and in dendritic arms (where they are 1.5–2 times smaller), and the γ-phase layer thickness (Fig. 2). The introduction of cobalt and rhenium into the VKNA-25 alloy was shown to decrease in the sizes of the structural components of all levels as compared to the VKNA-1V alloy (see Fig. 2). For example, the primary dendrite arm spacing in the VKNA-25 alloy is ~30% smaller than that in the VKNA-1V alloy, and the sizes of the structural components of the remaining levels in the VKNA-25 alloy are about 2–3 times smaller than those in the VKNA-1V alloy. An increase in the cooling rate of the ⟨001⟩ single crystals leads to a decrease in the sizes of the structural components of all levels in both alloys.

The effect of the cooling rate during the DS of alloy single crystals on the AE distribution between liquid and solid phases was studied (Fig. 3a). Distribution coefficient $k_d$ was determined as the ratio of the AE concentrations in solid and liquid phases ($c_S$ and $c_L$, respectively). $c_S$ was determined as the element con-

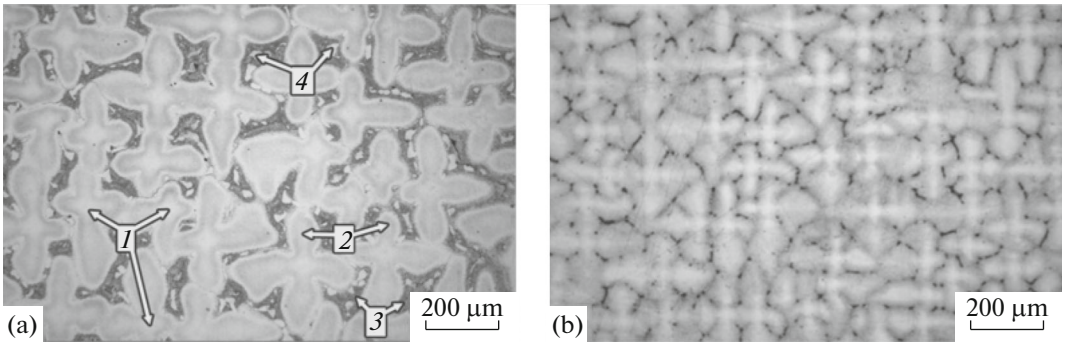


**Fig. 1.** Microstructure (OM) of the ⟨001⟩ single crystals of (a) VKNA-1V and (b) VKNA-25 alloys grown by high-gradient DS at a cooling rate of 150°C/min: (*1*, *2*) primary and secondary γ' + γ dendrite arms, respectively; (*3*) interdendritic space; and (*4*) primary γ'-$Ni_3Al$ precipitates in the interdendritic space.

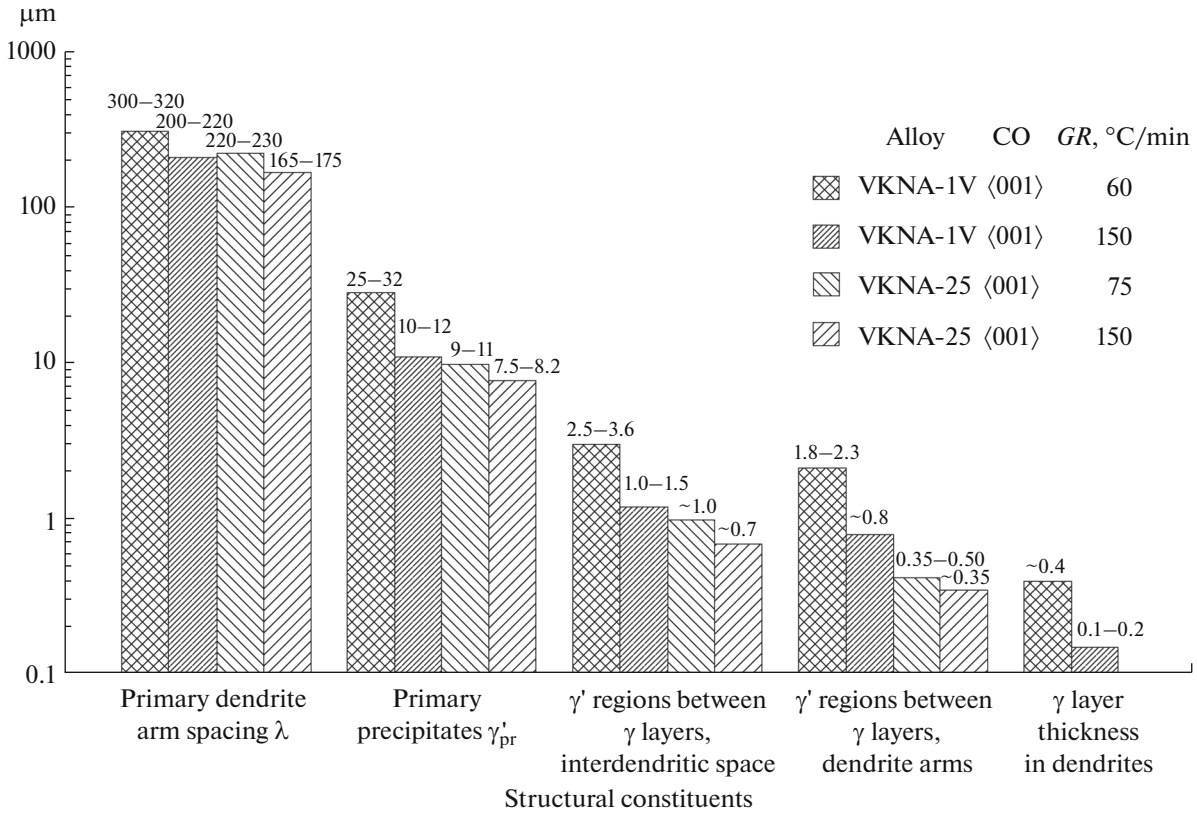


**Fig. 2.** Sizes of the structural constituents of the ⟨001⟩ VKNA-1V and VKNA-25 alloy single crystals grown by DS at various cooling rates.

centration in the primary dendrite arms $c_{d.a\text{-}I}$ in ⟨001⟩ single crystals or as $c_{d.a}$ in ⟨111⟩ single crystals, where primary and secondary dendrite arms alternate during solidification. The AE concentration in the liquid phase $c_L$, which corresponded to the alloy composition with a uniform element distribution in the melt, was designated as $c_0$. Thus, the distribution coefficients for the ⟨001⟩ and ⟨111⟩ single crystals are $k_d = c_{d.a\text{-}I}/c_0$ and $k_d = c_{d.a}/c_0$, respectively.

To quantitatively estimate the segregation characteristics in a dendritic cell, we used the dendritic microsegregation coefficients $k_s = c_{d.a\text{-}I}/c_{i.s}$ and $k_s = c_{d.a}/c_{i.s}$, where $c_{i.s}$ is the AE concentration in the interdendritic space (Fig. 3b).

As can be seen from Fig. 3, the rule derived for two- and three-component nickel-based alloys is fulfilled for both types of IM alloys based on γ'-$Ni_3Al$: the AE distribution coefficient is $k_d > 1$ if the introduced AE increases $T_m$ of the base metal (nickel). In addition, the greater the increase in the melting point, the more correct the fulfillment of this rule: Co ($k_d \approx 1.1$) → Re ($k_d \approx 1.25$) → W ($k_d \approx 1.35$). If an AE lowers the melting

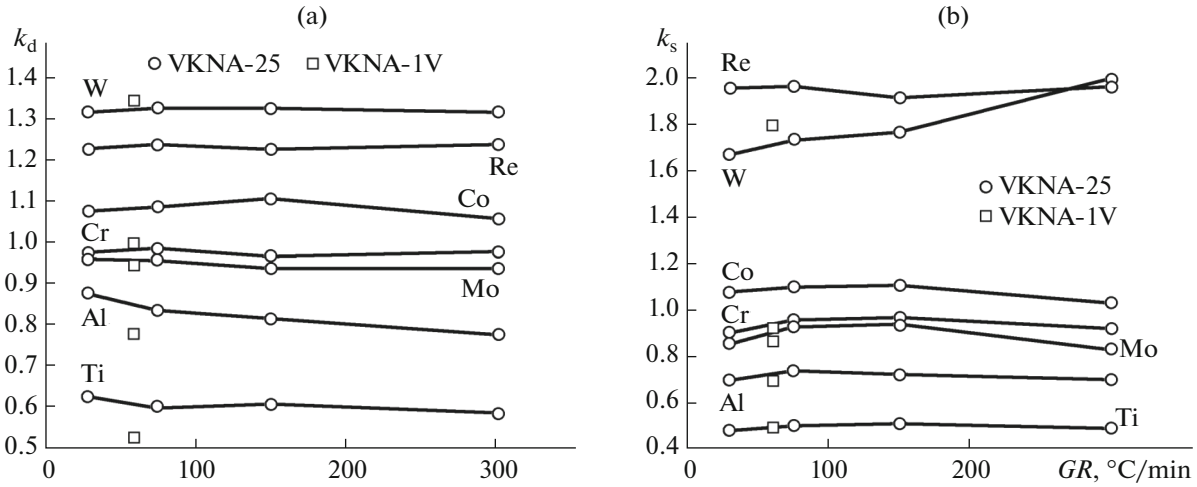


**Fig. 3.** Effect of the cooling rate during DS on the coefficients of (a) AE distribution and (b) dendritic microsegregation in the single crystals of VKNA-1V and VKNA-25 alloys.

point of nickel, we have $k_d < 1$: Mo (Cr) ($k_d \approx 0.98$) → Al ($k_d \approx 0.75$–$0.97$) → Ti ($k_d \approx 0.5$–$0.6$). It also follows from Fig. 3 that the distribution coefficients of all AEs except for aluminum are almost independent of the cooling rate; for the low-melting-point component (Al), the following clear dependence was revealed: $k_d$ decreases with increasing cooling rate. It is noteworthy that the AE distribution coefficient depends on the ratio of the AE contents in the alloys: for the VKNA-1V alloy (first type), coefficient $k_d$ of titanium and aluminum (relatively low melting temperature) is significantly lower than that for the alloy of the second type with 4.5 wt % Co and 1.6 wt % Re. This fact is due to the complex effect of AEs on temperature $T_{solidus}$ in a multicomponent alloy. The dendritic microsegregation coefficients $k_s$ of all AEs except for tungsten only weakly depend on the cooling rate and decrease in the following row (Fig. 3b): Re ($k_s \approx 2$), Co ($k_s \approx 1.1$), Mo ($k_s \approx 0.9$), Al ($k_s \approx 0.7$), and Ti ($k_s \approx 0.5$). For tungsten, $k_s$ increases from ~1.7 for $GR = 30$°C/min to ~2 for $GR = 300$°C/min. A weak tendency toward a decrease in $k_s$ for cobalt, chromium, and molybdenum is also worth noting.

### *Cast Alloys: Mechanical Properties*

The strength and plasticity characteristics in the temperature range 20–1200°C were studied on the single crystals of alloys of the first and second types (VKNA-1V and VKNA-25, respectively), the cooling rate of which during DS was 60–80°C/min (Fig. 4).

As is seen from Fig. 4, the alloys have fairly high strength and heat-resistance characteristics; however, the scatter of the characteristics is quite large because of the internal stresses that appear during solidification in single crystals and the stresses caused by mechanical processing during sample preparation. We performed short- and long-term HT over a wide temperature range to remove these stresses and to study the effect of HT on the microsegregation parameters, the structural-phase state, and the mechanical properties of the alloys of the first (VKNA-1V) and second (VKNA-25) types.

### *HT Conditions*

The HT temperature ranges were selected on the basis of the studies conducted in 2018–2020 [21, 32] (Table 2).

**Table 2.** HT conditions for VKNA-1V and VKNA-25 alloys

| HT | Temperature range | *T*, °C | HT time, h |
|---|---|---|---|
| HT1 | $T < T_{solvus}$* | 1000–1200 | 1–2 (short-term HT) |
| HT2 | $T < T_{solvus}$ | 1000 | 25, 50, 100 (long-term HT) |
| HT3 | $T \geq T_{solvus}$ | 1200–1280 | 5, 10, 100, 250, 500 |
| HT4 | $T_{solvus} \leq T \leq T_{solidus}$** | 1300 | 10 |

* $T_{solvus}$ is the temperature of $\gamma'_{sec}$-phase precipitation from the nickel-based supersaturated solid solution ($\gamma$ phase) forming layers between $\gamma'$ regions in dendrites.

** $T_{solidus}$ is the temperature of the $L \rightleftarrows \gamma' + \gamma$ eutectic transformation, which can vary in the range 1330–1350°C for VKNA-type alloys.

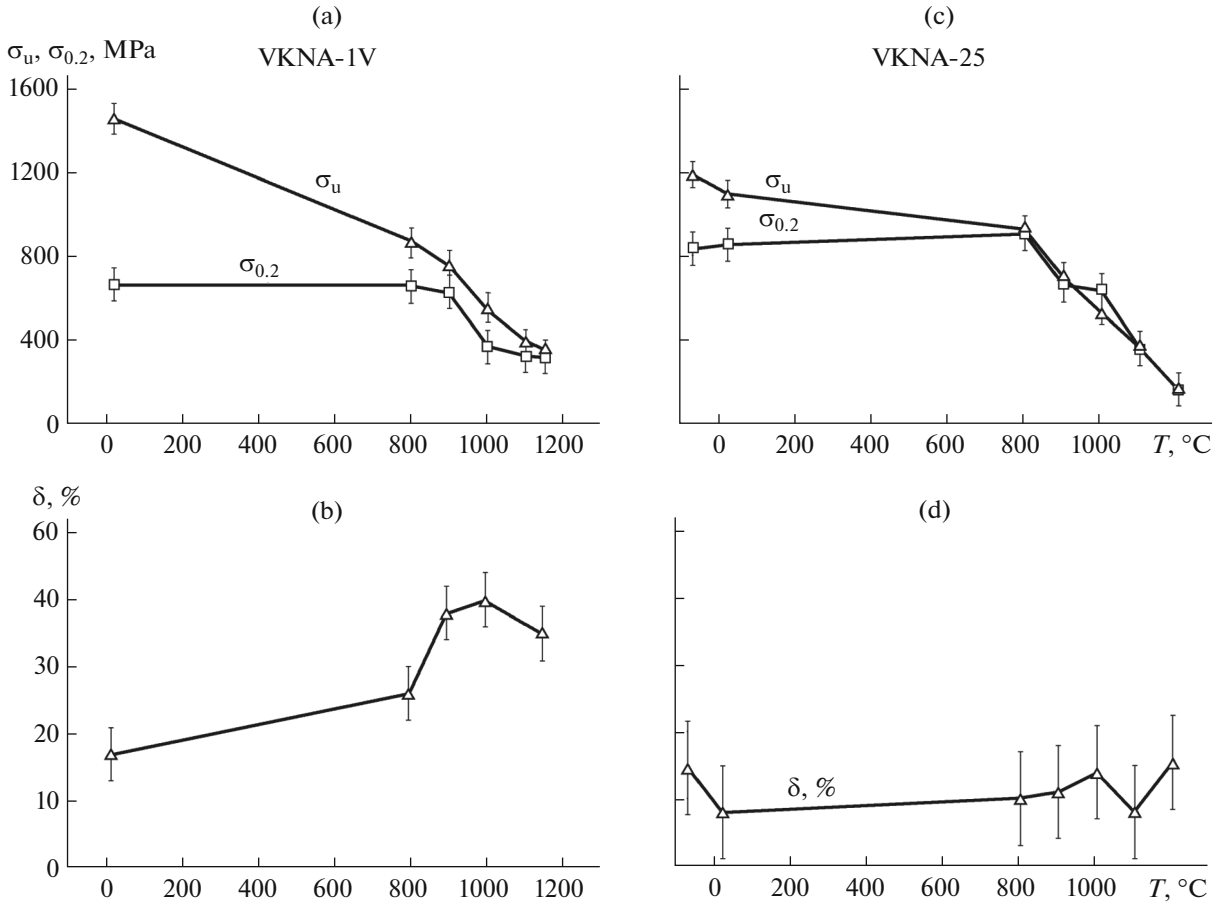


**Fig. 4.** Effect of temperature on the strength ($\sigma_u$, $\sigma_{0.2}$) and plasticity (δ) characteristics of the as-cast ⟨111⟩ single crystals of (a, b) VKNA-1V and (c, d) VKNA-25 (with Co and Re) alloys.

Table 3 gives data on the influence of HT on the dendritic microsegregation coefficient $k_s$ of the main AEs in the VKNA-25 alloy single crystals at $GR$ = 150°C/min, since it contains AEs (Co, Re), which are not involved in the VKNA-1V alloy, in addition to the main AE set (Al, Ti, Cr, Mo, W).

It should be noted that the dendritic microsegregation coefficients after HT1 (see Table 3) are close to those in the state after DS. After short- and long-term HT of the VKNA-25 alloy single crystals at temperatures below $T_{solvus}$, the dendritic microsegregation coefficients change slightly.

Short- and long-term annealing at $T > T_{solvus}$ according to the HT3 conditions practically eliminates the dendritic microsegregation of most AEs: the dendritic microsegregation coefficients of low-melting (Al), the most refractory AE (W), and Cr, Co, and Mo in the VKNA-25 alloy single crystals become equal to unity; the exceptions are Ti ($k_s$ = 0.85) and Re ($k_s$ = 1.3). After long-term (10 h) annealing at $T \le T_{solidus}$

**Table 3.** Effect of HT on the dendritic microsegregation coefficient $k_s = c_{d.a}/c_{i.s}$ of the main AEs in the VKNA-25 alloy single crystals, $GR$ = 150°C/min

| State of alloy | Al | Ti | Cr | Co | Mo | W | Re |
|---|---|---|---|---|---|---|---|
| DS | 0.90 | 0.50 | 0.90 | 1.10 | 0.90 | 1.80 | 2.2 |
| DS + HT1 (1100°C, 2 h) | 0.90 | 0.50 | 0.95 | 1.08 | 0.90 | 1.70 | 2.0 |
| DS + HT2 (1000°C, 100 h) | 0.95 | 0.65 | 0.95 | 1.03 | 0.93 | 1.65 | 1.8 |
| DS + HT3 (1250°C, 100 h) | 1.00 | 0.85 | 1.00 | 1.00 | 0.97 | 1.15 | 1.3 |
| DS + HT4 (1300°C, 10 h) | 1.00 | 0.90 | 1.00 | 1.05 | 1.00 | 1.00 | 1.3 |

The values were averaged over at least 15 measurements and the scatter of the values did not exceed ±3%.

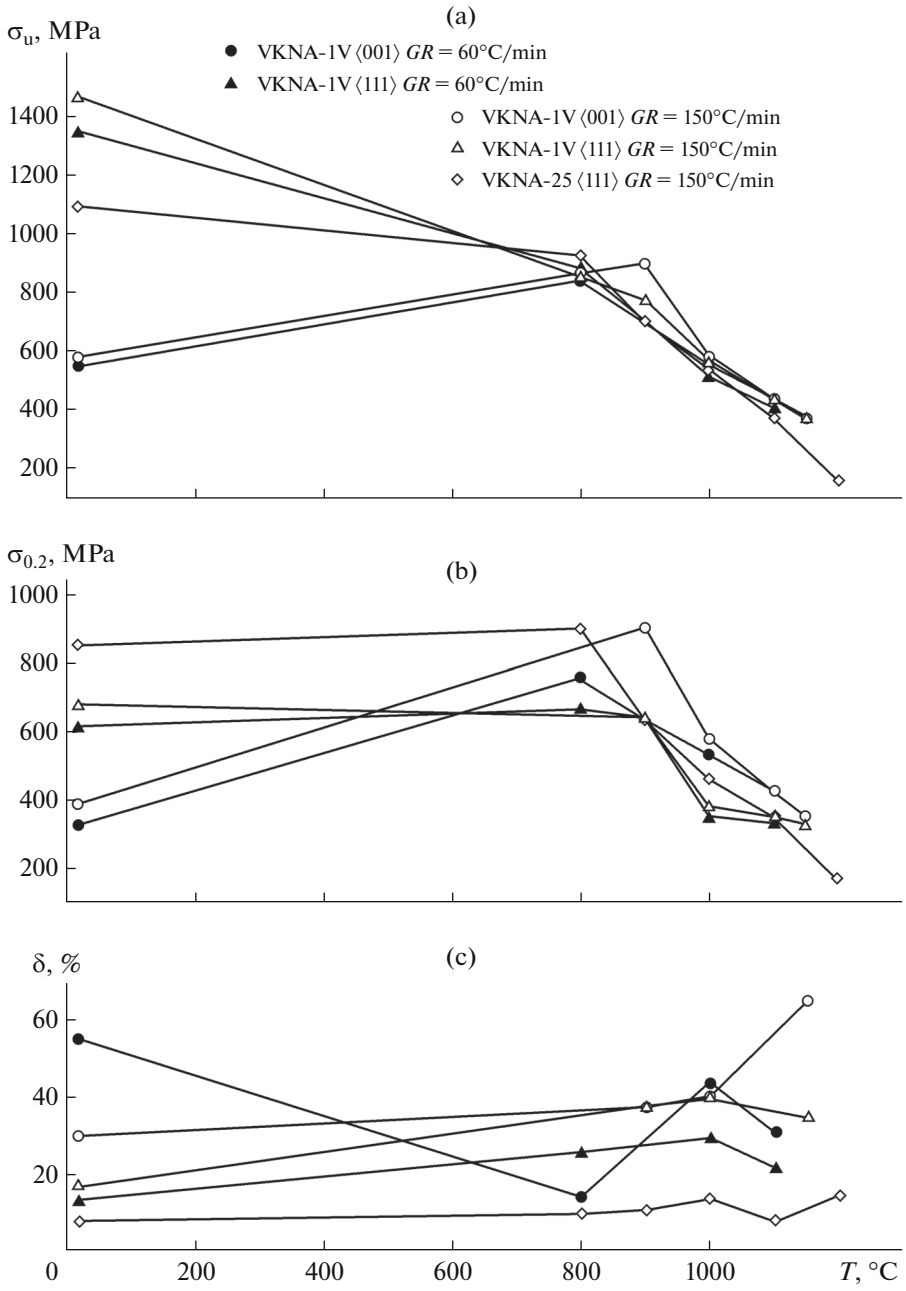


**Fig. 5.** Effect of test temperature $T$ on (a) ultimate tensile strength $\sigma_u$, (b) yield strength $\sigma_{0.2}$, and (c) elongation $\delta$ of the ⟨001⟩ and ⟨111⟩ VKNA-1V and VKNA-25 alloys grown by DS at cooling rates $GR$ = 60 and 150°C/min. Heat treatment according to schedule HT1.

(HT4), we have $k_s \approx 1$ for all AEs except for rhenium, which mainly enriches dendrite arms, since it dissolves only in γ layers and does not dissolve in coarse primary γ′-phase precipitates located in the interdendritic space.

The influence of short-term (1–2 h) HT (HT1 schedule) at temperatures $< T_{solvus}$ (1000, 1100, 1150, 1200°C) on the structure, short-term strength, durability, and fracture was studied on the single crystals of both types of alloys formed by DS at a cooling rate $GR$ = 60 and 150°C/min. The temperature dependences of the strength and plasticity characteristics of the single crystals with the basic COs are shown in Fig. 5.

As is seen from Fig. 5, an increase in the cooling rate by 2.5 times (from 60 to 150°C/min) increases the ultimate tensile strength and the yield strength of the VKNA-1V alloy at room temperature $T_r$. For example, $\sigma_u$ of the ⟨001⟩ single crystals increases from 550 to ~600 MPa, and $\sigma_u$ of the ⟨111⟩ single crystals increases

from 1350 to 1470 MPa, which is associated with the refinement of structural components (see Fig. 2). At temperatures of 1000–1150°C, the ultimate tensile strengths of the single crystals with different COs and solidification rates are close and depend on the cooling rate to a lesser extent. For example, $\sigma_u$ of the ⟨001⟩ and ⟨111⟩ single crystals increases from 520–550 MPa for $GR$ = 60°C/min to 570–580 MPa for $GR$ = 150°C/min (Fig. 5a). The general tendency is as follows: at temperatures above 1100°C, the single crystals of the second type (VKNA-25, ⟨111⟩ CO) soften faster than the single crystals of the first type (VKNA-1V) with any CO (Figs. 5a, 5b).

It should also be noted that the slight decrease in the dendritic microsegregation coefficients in the VKNA-25 alloy single crystals after HT1 (see Table 3) weakly affects the heat-resistance characteristics of the alloy as compared to those for the starting material after DS (see Figs. 4 and 5).

The presence of a strong anomaly in the temperature dependence of the strength characteristics of the ⟨001⟩ VKNA-1V alloy single crystals grown at cooling rates at $GR$ = 60 and 150°C/min during solidification, namely, the maximum at 800–900°C, is noteworthy. At the same time, for $GR$ = 150°C/min, yield strength $\sigma_{0.2}$ increases from 390 MPa at $T_r$ to 905 MPa at 900°C. For the ⟨111⟩ single crystals of both alloys, this anomaly manifests itself but in the absence of softening in the temperature range 800–900°C (yield strengths at $T_r$ and 800–900°C are almost the same) rather than in an increase in the strength characteristics when the temperature increases from $T_r$ to 800–900°C (see Figs. 4a, 4c). This difference is due to a change in the slip systems during the transition through the temperature of the peak yield and strength (near 800°C). The change of the octahedral slip to the cubic one with increasing temperature was revealed in many IM alloys with the $L1_2$ superstructure (including $Ni_3Al$), the $L1_0$ superstructure (TiAl), and some other superstructures [15, 38]. The elongation of the ⟨111⟩ single crystals of both alloys at $T_r$ is significantly smaller than that of the ⟨001⟩ VKNA-1V alloy single crystals and increases gradually with temperature. The elongation of the VKNA-25 alloy single crystals is approximately 2–2.5 times smaller than that of the VKNA-1V alloy. The ⟨001⟩ VKNA-1V alloy single crystals grown at $GR$ = 60°C/min are characterized by a nonmonotonic temperature dependence of the elongation: a plasticity dip at the temperatures of the peak ultimate strength and yield strength (800–900°C). The plasticity dip was not detected for the ⟨001⟩ VKNA-1V alloy single crystals grown at $GR$ = 150°C/min, which can be due to a decrease in the phase and structural-component sizes (see Fig. 2).

The structure and the fracture of the VKNA-1V and VKNA-25 single crystals (after HT1) at room temperature $T_r$ are shown in Fig. 6, and those at 1000°C, in Figs. 7a and 7b.

As is seen from Figs. 6a and 6e, the fracture of the alloys of both the first and second types during short-term tests at $T_r$ is not accompanied by surface cracking and does not lead to a change in the microstructure in the rupture zone. The absence of transverse cracks ("breaks") in the neck area indicates the absence of stress localization at any structure elements and the presence of strong bonding between them. Despite the high plasticity characteristics (uniform deformation ability), the fracture occurs crystallographically along the octahedral {111} slip planes. In the alloy of the second type after HT1, two-phase γ′ + β primary precipitates are retained in the interdendritic space (Figs. 6d–6f).

The effect of schedule HT1 the structure and fracture at 1000°C is shown in Fig. 7 for the VKNA-25 alloy. The fundamental difference in the character of fracture at 1000°C during short-term (Figs. 7a, 7b) and long-term (Fig. 7d, 7e) action of stresses is worth noting. Rare transverse cracks (breaks) form near the fracture zone in the VKNA-25 alloy after HT1 during short-term tensile tests at 1000°C. Traces of crack initiation can hardly be seen on the sample surface (see Fig. 7a). Elements of ductile fracture (fracture ridges; see Figs. 7b, 7c) and crystallographic fracture (see Fig. 7a) are combined. Two-phase γ′ + β primary precipitates are retained in the interdendritic space (see Fig. 7b). Elongated γ′-particle regions are observed in dendrite arms (see Fig. 7c). When the VKNA-25 alloy is subjected to durability tests at 1000°C, numerous deep transverse cracks form on the sample surface (Fig. 7d). The fracture surface is mixed: numerous (including large) transverse cracks are visible near the fracture zone (see breaks in Figs. 7d, 7e), and small rounded pores, which do not form during short-term tests, appear (Figs. 7d, 7e). The coarse interdendritic precipitates become single-phase γ′ phase), and the nonequilibrium β-phase precipitates disappear (Fig. 7f).

The study of the influence of the temperature of short-term annealing for 1 h (HT1 schedule) on the durability at 1000°C of ⟨111⟩ VKNA-1V alloy single crystals showed that the long-term strength characteristics changed nonmonotonically with increasing HT temperature: the highest characteristics were obtained on the samples annealed at 1150°C for 1 h (Fig. 8). The alloys are in a nonequilibrium structural-phase state. For example, two-phase primary γ′ + β precipitates are retained in the interdendritic space in the VKNA-25 alloy samples after HT1. An increase in the short-term annealing temperature to 1200°C leads to a certain decrease in the strength and durability of the single crystals of both types of alloys.

This fact indicates that the process is influenced by several different factors. First of all, the casting stresses that appear in the single crystals during DS and mechanical processing of samples are removed during short-term annealing. This process begins at 1050°C

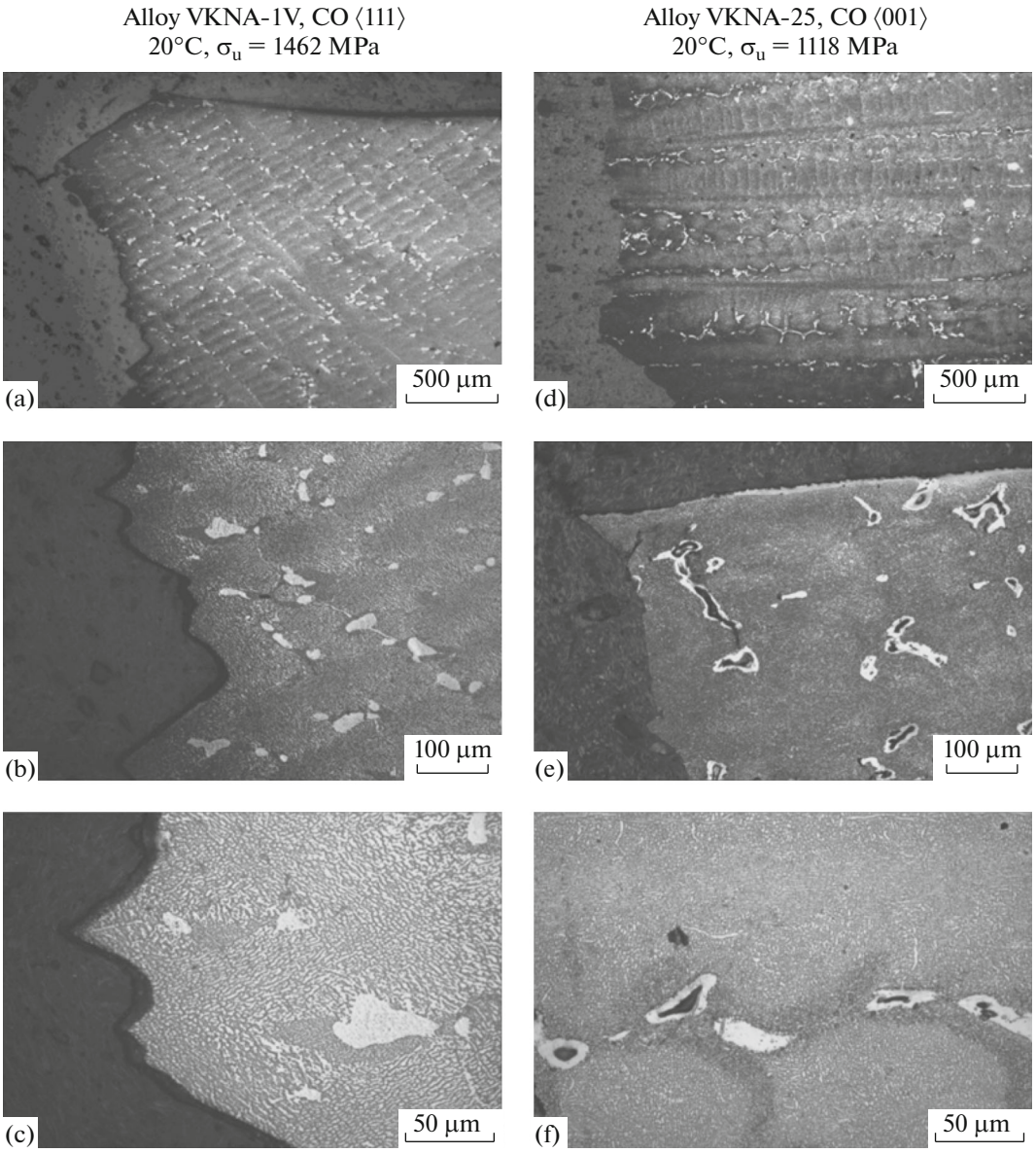


**Fig. 6.** Microstructures (OM) of the fracture zone at $T_r$ of alloys (a–c) VKNA-1V and (d–f) VKNA-25 treated according to schedule HT1.

and reaches a maximum at 1150°C. In parallel, diffusion processes aimed at reducing the dendritic microsegregation develop on heating (see Table 3). When the HT temperature increases, the dendritic microsegregation coefficient of almost all elements (except for rhenium) tends toward unity. This leads to a certain change in the volume fraction of the phases, their composition, and, consequently, the lattice parameters, which, in turn, affects the mismatch of the γ′- and γ-phase lattices and the heat-resistance characteristics.

The effect of long-term HT at 1000°C for 25, 50 and 100 h (HT2 schedule) and at 1200–1300°C for 10 h (HT3, HT4 schedules) on durability was studied on the single crystals grown during DS at a cooling rate $GR = 150$°C/min.

Using the VKNA-1V alloy as an example, we showed that the durability of the alloy decreases when the HT time (at 1000°C) increases to 100 h at $T < T_{solvus}$ (Fig. 9a). This is due to the structural-phase changes induced by a decrease in the dendritic microsegregation, as discussed above. The study of the effect of increase in the temperature of 10-h HT to 1300°C on the structure and durability, which was carried out on the VKNA-25 alloy (Fig. 9b) showed that the volume fraction of primary γ′-phase precipitates in the interdendritic space decreases (almost disappears) with increasing HT temperature (Fig. 9b).

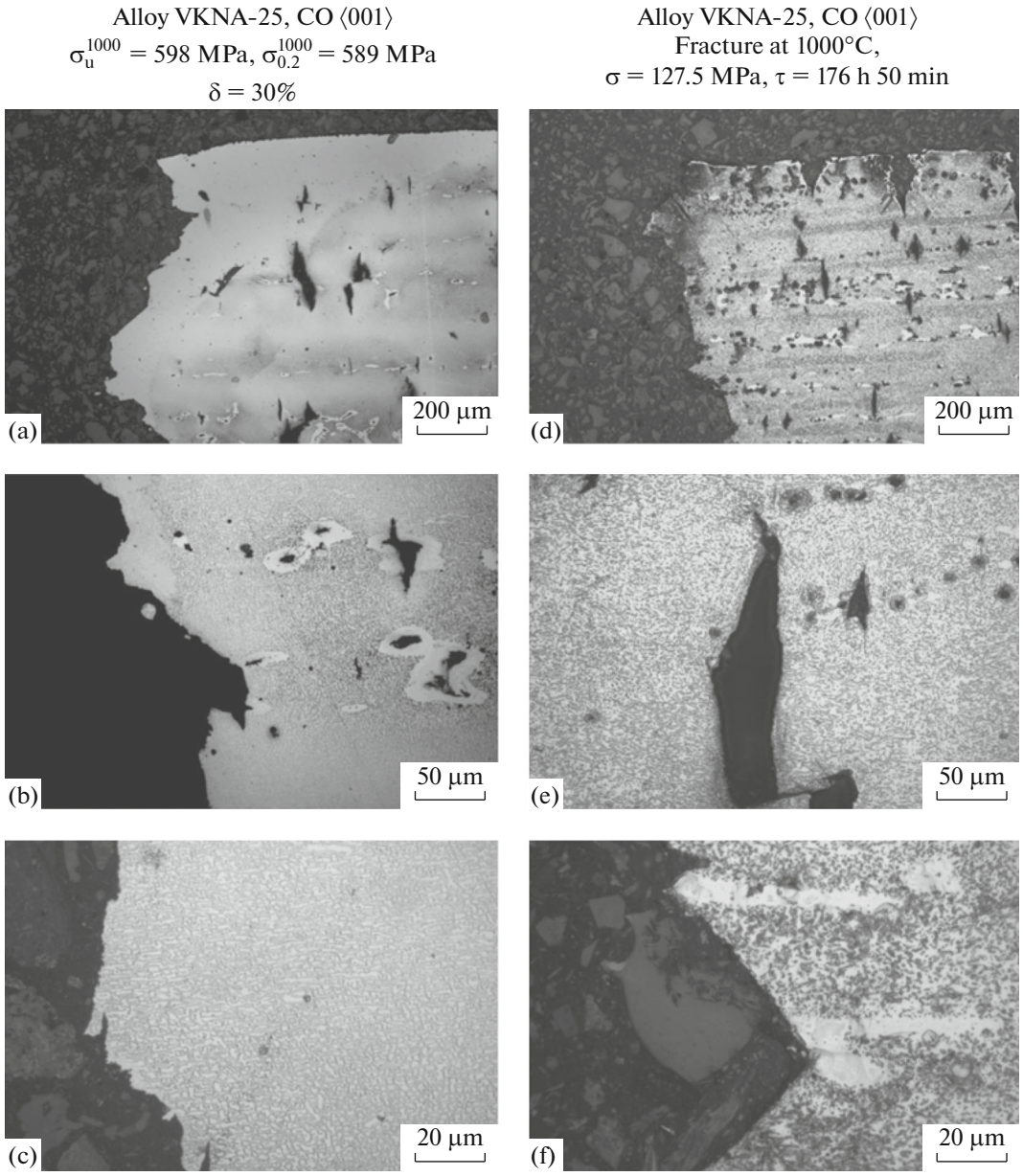


**Fig. 7.** Microstructures (OM) of the fracture zone at $T = 1000$°C of the ⟨001⟩ VKNA-25 alloy after (a–c) short–term and (d–f) long-term (durability) tests.

The structure of both alloys becomes almost homogeneous and consists of rather large γ′-phase areas of irregular shape surrounded by continuous or discontinuous γ-phase layers. This process can be called "homogenization" of heterophase γ′ + γ IM alloys. This behavior correlates with the data in Table 3, according to which the dendritic microsegregation coefficients of all elements change and tend toward $k_s \approx 1$ for all AEs except for rhenium, which enriches dendrite arms [32], with increasing HT temperature or time.

In this case, the durability of the alloy becomes almost three times lower than that of the alloy annealed according to the optimum schedule (1150°C, 1 h), which is characterized by the maximum microsegregation heterogeneity.

An increase in the temperature to 1200–1300°C and an increase in the HT time to 5–500 h cause different degrees of structure homogenization. The nonequilibrium β phase disappears, the volume fraction of coarse primary γ′-phase precipitates in the interdendritic space decreases strongly, and AEs are redistributed between dendrite arms and the interdendritic space (dendritic microsegregation coefficients of all elements tend toward $k_s \approx 1$).

This homogenization brings about a decrease in the high-temperature durability of the single crystals of

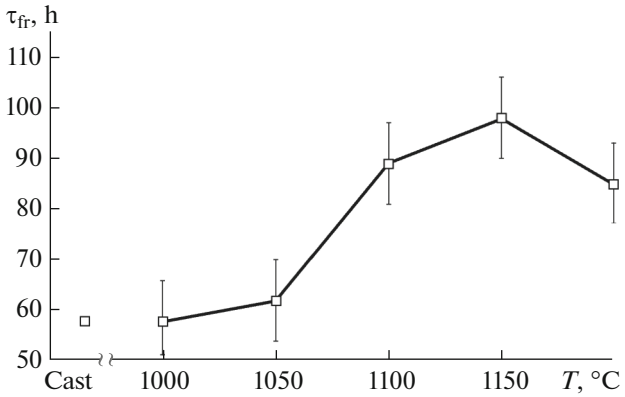


**Fig. 8.** Effect of the temperature of short-term annealing for 1 h (HT1 schedule) of the ⟨111⟩ VKNA-1V alloy single crystals on the durability at 1000°C and σ = 180 MPa ($\tau_{fr}$ is time to failure).

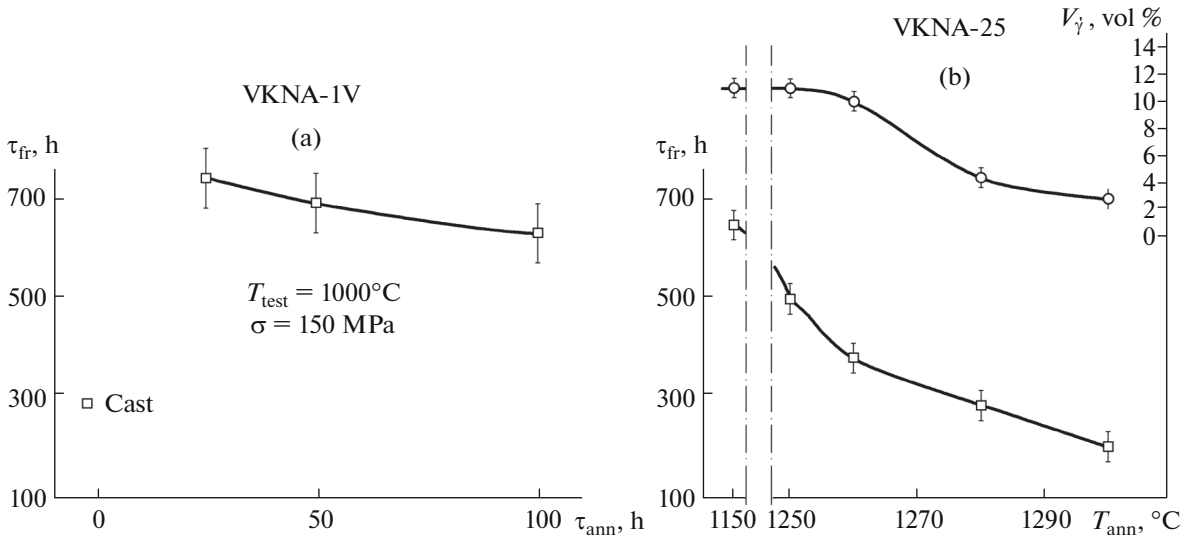


**Fig. 9.** Effect of (a) time of annealing at 1000°C (HT2) on the durability of the ⟨111⟩ VKNA-1V alloy single crystals at a temperature of 1000°C and a stress of 150 MPa and (b) temperature of 10-h treatment according to schedules HT3 and HT4 on the volume fraction $V_{\gamma'}$ of primary γ'-phase precipitates and the durability at 1100°C and σ = 50 MPa of the ⟨001⟩ VKNA-25 alloy.

both types of alloys. For example, the durability of the VKNA-25 alloy after the so-called homogenization becomes ~3 times lower than that of the alloy single crystal annealed according to the optimum schedule (1150°C, 1 h), which is characterized by the maximum microsegregation heterogeneity (Fig. 9b).

The homogeneous γ' + γ structure formed in the IM alloys, which is characteristic of IM dendrites (irregular γ'-phase regions separated by continuous or discontinuous γ-phase layers; Fig. 10a), is fundamentally different from the structure of NSA (Fig. 10b).

Long-term homogenization in the single-phase γ solid solution field of NSA and subsequent alternation of dissolution–aging cycles allow the formation of homogeneous heterophase $\gamma + \gamma'_{sec}$ structures, which are responsible for the high heat-resistance characteristics of NSAs with specified morphology (cuboids) and sizes of fine particles of the hardening $\gamma'_{sec}$ phase of various genesis and the optimum γ/γ' misfit.

Thus, the results of this stage of work demonstrate that short-term (1–2 h) annealing at 1150°C can be used to improve the strength and heat-resistance characteristics of VKNA-1V and VKNA-25 alloy single crystals with the basic COs; this annealing weakly changes the structure of the alloys. However, this investigation does not address the structural changes occurring at a deep level, such as changes in the dislocation structure during HT and the composition, size, and formation of additional phases in multicomponent alloys.

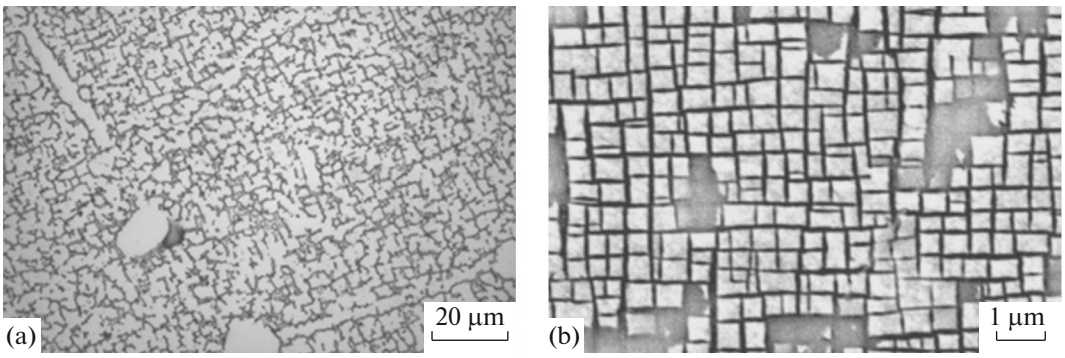


**Fig. 10.** (a) Microstructure of the VKNA-25 IM alloy after homogenizing annealing at 1300°C for 10 h and (b) characteristic microstructure of the NSA alloy after treatment according to the traditional FGUP VIAM scheme for NSA.

## CONCLUSIONS

(1) We studied the influence of the temperature–time parameters (temperature from 1000 to 1300°C, time from 1 to 500 h) of HT of ⟨001⟩ and ⟨111⟩ single crystals of boron-free heterophase γ'-$Ni_3Al$ + γ-Ni IM alloys of the first (VKNA-1V) and second (VKNA-25, with cobalt and rhenium) types on their structure, fracture, and short-term and long-term strength.

(2) The introduction of cobalt and rhenium in the VKNA-25 alloy was found to decrease the sizes of the structural components of all levels as compared to the VKNA-1V alloy: the primary dendrite arm spacing in the VKNA-25 alloy is ~30% smaller than that in the VKNA-1V alloy, and the sizes of the structural components of the remaining levels in the VKNA-25 alloy are about 2–3 times smaller than those in the VKNA-1V alloy. An increase in the cooling rate of the ⟨001⟩ single crystals in the range 30–300°C/min leads to a decrease in the sizes of the structural components of all levels in both alloys.

(3) The rule derived for two- and three-component nickel-based alloys was found to be fulfilled for the IM alloys based on γ'-$Ni_3Al$: if the introduced AE increases the melting temperature $T_m$ of the base metal (nickel), the AE distribution coefficient is $k_d > 1$ and the AE enriches dendrite arms; the higher the melting point of AE, the higher the degree of enrichment, Co ($k_d \approx 1.1$) → Re ($k_d \approx 1.25$) → W ($k_d \approx 1.35$). If an AE decreases the melting point of nickel, we have $k_d < 1$ (AE enriches the interdendritic space): Mo, Cr ($k_d \approx 0.98$) → Al ($k_d \approx 0.75$–$0.97$) → Ti ($k_d \approx 0.5$–$0.6$).

(4) The dendritic microsegregation coefficients $k_s$, which characterize the nonuniform AE distribution in the dendritic–cellular structure of the single crystals, were found to weakly depend on the cooling rate and to decrease in the following row: Re ($k_s \approx 2$), Co and Mo ($k_s \approx 0.9$), Al ($k_s \approx 0.7$), and Ti ($k_s \approx 0.5$). For tungsten, $k_s$ increases from ~1 for $GR = 30$°C/min to ~2 for $GR = 300$°C/min.

(5) An increase in the time of low-temperature HT ($T < T_{solvus}$) and an increase in the HT temperature to $T_{solvus} \le T \le T_{solidus}$ leads to the homogenization of the heterophase γ + γ' IM alloys. The dendritic microsegregation coefficients of all AEs (except for Re) approach unity, and primary $\gamma'_{pr}$-phase precipitates and nonequilibrium γ' + β precipitates in the interdendritic space disappear. A homogeneous heterophase γ' + γ structure, which is typical of IM dendrites (γ'-phase regions are separated by continuous or discontinuous γ-phase layers), forms.

This structure differs from that of NSAs.

(6) The homogenization of this type gives rise to a decrease in the durability as compared to the as-cast material, which retains the maximum microsegregation heterogeneity after short-term HT performed to relieve casting stresses.

## FUNDING

This work was performed according to state assignment no. 075-00746-19-00 and was supported by the Russian Foundation for Basic Research (project no. 19-03-00852_a).

## REFERENCES

1. R.C. Reed, *The Superalloys: Fundamentals and Applications* (Cambridge University Press, Cambridge, 2008).
2. T. Sims, S. Stoloff, and C. Hagel, *Superalloys II: High-Temperature Materials for Aerospace and Industrial Power* (New York, 1987).
3. E. N. Kablov and E. R. Golubovskii, *Heat Resistance of Nickel Alloys* (Mashinostroenie, Moscow, 1998).
4. E. N. Kablov, N. E. Petrushin, and I. L. Svetlov, "Modern cast high-temperature nickel alloys," in *Proceedings of Conference Dedicated to the 100th Anniversary of the Birth of S.T. Kishkin* (VIAM, Moscow, 2006), pp. 39–55.
5. *Cast Blades of Gas Turbine Engines: Alloys, Technology, Coatings*, Ed. by E. N. Kablov (Nauka, Moscow, 2006).

6. E. N. Kablov, B. S. Lomberg, V. P. Buntushkin, E. P. Golubovskii, and S. A. Muboyadzhyan, "Intermetallic $Ni_3Al$-base alloy: a promising material for turbine blades," Metal Sci. Heat Treat. **44** (7–8), 284–287 (2002).
7. K. B. Povarova, N. K. Kazanskaya, V. P. Buntushkin, V. G. Kostogryz, V. G. Bakharev, V. I. Mironov, O. A. Bazyleva, A. A. Drozdov, and I. O. Bannykh, "Thermal structural stability of an $Ni_3Al$-based alloy and its application for blades in small gas-turbine engines," Russ. Metall. (Metally), No. 3, 269–274 (2003).
8. K. B. Povarova, A. A. Drozdov, V. P. Buntushkin, N. K. Kazanskaya, and O. A. Bazyleva, "Ultralight heat-resistant nanostructured alloys based on $Ni_3Al$ for aircraft engine building and power engineering," Vopr. Materialoved., No. 2 (54), 85–93 (2008).
9. N. A. Nochovnaya, O. A. Bazyleva, D. E. Kablov, and P. V. Panin, *Intermetallic Alloys Based on Titanium and Nickel*, Ed. by E. N. Kablov (VIAM, Moscow, 2018).
10. S. M. Seo, J. H. Lee, Y. S.Yoo, Jo. H. Miyahara, and R. Ogi, "A comparative study of the $\gamma/\gamma'$ eutectic evolution during the solidification of Ni-base superalloys," Met. Mater. Trans. A **42**, 3150–3159 (2011).
11. H. T. Pang, H. B. Dong, R. Beanland, H. J. Stone, C. M. F. Rae, P. A. Midgley, G. Brewster, and N. D'Souza, "Microstructure and solidification sequence of the interdendritic region in a third generation single-crystal nickel-base superalloy," Met. Mater. Trans. A **40**, 1660–1669 (2009).
12. N. S. Stoloff, "Physical and mechanical metallurgy of $Ni_3Al$ and its alloys," Int. Mater. Rev. **34** (1), 150–183 (1989).
13. M. Nazmy and M. Staubli, "Aspects of mechanical behaviour of directional solidified $Ni_3Al$ intermetallics," Scr. Metall. **25** (6), 1305–1308 (1991).
14. D. J. Alexander and V. R. Sicca, "Mechanical properties of advanced nickel aluminides," Mater. Sci. Eng. A **152**, 114–119 (1992).
15. C. T. Liu, "$Ni_3Al$ aluminide alloys," in *Structural Intermetallics*, Ed. by R. Darolia, J. J. Lewandowski, et al. (Miner. Metals Mater. Soc., 1993), pp. 365–377.
16. K. Aoki and O. Izumi, J. Jap. Inst. Met. **43**, 1190 (1979).
17. Y. F. Han, S. H. Li, and V. C. Chaturvedi, "Microstructural stability of the directionally solidified $\gamma'$-base superalloy IC6," Mater. Sci. Eng. **160**, 271–276 (1993).
18. V. P. Buntushkin, O. A. Bazyleva, K. B. Povarova, and N. K. Kazanskaya, "Effect of structure on the mechanical properties of alloyed $Ni_3Al$ intermetallic compound," Metals, No. 3, 74–80 (1995).
19. *Intermetallic Alloy Development. A Program Evaluation Panel of Intermetallic Alloy Development Committee on Industrial Technology Assessments, National Materials Advisory Board. Commission on Engineering and Technical Systems. National Research Council. Publ. NMAB-487-1* (National Academy Press, Washington, 1997).
20. K. B. Povarova and O. A. Bannykh, "Principles of creating structural alloys based on intermetallics," Materialoved., No. 2, 27–33 (1999); No. 3, 29–37 (1999).
21. K. B. Povarova, A. A. Drozdov, O. A. Bazyleva, M. A. Bulakhtina, A. E. Morozov, A. V. Antonova, E. G. Arginbayeva, and Yu. V. Loshchinin "Solidification and structure-phase state of $Ni_3Al$–Ni–NiAl alloys with chromium, molybdenum, tungsten, rhenium, and cobalt," Russ. Metall. (Metally), No. 5, 540–548 (2020).
22. Ai Cheng, Xinbao Zhao, Lei Liu, Heng Zhang, Yi Ru, Yanling Pei, Jian Zhou, Shusuo Li, and Shengkai Gong, "Influence of withdrawal rate on last solidification path of a Mo-rich $Ni_3Al$ based single crystal superalloy," J. Alloys Comp. **623**, 362–366 (2015).
23. Y. F. Han and C. B. Xiao, "Effect of yttrium on microstructure and properties of $Ni_3Al$ base alloy IC6," Intermetallics **8** (6), 687–691 (2000).
24. Y. Cheng, H. Zhang, L. W. Song, et al., "Effect of Re element on oxidation resistance of $Ni_3Al$–Mo based alloys at 1150°C," Trans. Nonfer. Metal Soc. China **22** (3), 510–515 (2012).
25. *Academic Committee of the Superalloys CSM. China Superalloys Handbook (Book 2)* (China Quality and Standards Publ., Beijing, 2012).
26. Xiong Yue, Fengmei Liu, Qi Li, Hongbo Qin, Haitao Gao, Likun Li, and Yaoyong Yi, "Effect of post-bond heat treatment on microstructure and mechanical properties of the wide gap TLP bonded IC10 superalloy with a low boron $Ni_3Al$-based interlayer," J. Manufact. Proc. **54**, 109–119 (2020).
27. Shuaiqi Zhang, Zhongxue Yang, Ruisong Jiang, Qichao Jin, Qiang Zhang, and Wenhu Wang, "Effect of creep feed grinding on surface integrity and fatigue life of $Ni_3Al$ based superalloy IC10," Chin. J. Aeronaut. **34** (1), 438–448 (2020).
28. Jing Wu, Chong Li, Liu Yongchang, Xia Xingchuan, Zixiang Zheng, and Haipeng Wang, "Precipitation of intersected plate-like $\gamma'$ phase in $\beta$ and its effect on creep behavior of multiphase $Ni_3Al$-based intermetallic alloy," Mater. Sci. Eng. A **767**, 138439 (2019).
29. Jing Wu, Chong Li, Yongchang Liua, Xingchuan Xia, Yuting Wu, Zongqing Ma, and Haipeng Wang, "Influences of solution cooling rate on microstructural evolution of a multiphase $Ni_3Al$-based intermetallic alloy," Intermetallics **109**, 48–59 (2019).
30. K. B. Povarova, A. A. Drozdov, Yu. A. Bondarenko, O. A. Bazyleva, M. A. Bulakhtina, A. E. Morozov, and A. V. Antonova, "Effect of directional solidification on the structure and properties of $Ni_3Al$-based alloy single crystals alloyed with W, Mo, Cr, and REM," Russ. Metall. (Metally), No. 7, 532–536 (2014).
31. K. B. Povarova, Yu. A. Bondarenko, A. A. Drozdov, O. A. Bazyleva, A. V. Antonova, A. E. Morozov, and E. G. Arginbayeva, "Effect of directional solidification on the structure and properties of $Ni_3Al$-based alloy single crystals alloyed with Cr, Mo, W, Ti, Co, Re, and REM," Russ. Metall. (Metally), No. 1, 43–50 (2015).
32. K. B. Povarova, O. A. Bazyleva, A. A. Drozdov, A. E. Morozov, E. G. Arginbaeva, and A. V. Antonova, "Effect of heat treatment on dendritic segregation and high-temperature strength of single crystals of $Ni_3Al$-

base rhenium-alloyed intermetallic alloys", Metal Sci. Heat Treat. **60** (9–10), 594–601 (2019).

33. A. A. Drozdov, K. B. Povarova, A. E. Morozov, A. V. Antonova, and M. A. Bulakhtina, "Dendrite segregation in $Ni_3Al$-based intermetallic single crystals alloyed with Cr, Mo, W, Ti, Co, and Re," Russ. Metall. (Metally), No. 7, 551–557 (2015).
34. Ai Cheng, Li Shusuo, Heng Zhang, Lei Liu, Yue Ma, Yanling Pei, and Shengkai Gong, "Effect of withdrawal rate on microstructure and lattice misfit of a $Ni_3Al$ based single crystal superalloy," J. Alloys Comp. **592** (15 April), 164–169 (2014).
35. O. A. Bazyleva, K. B. Povarova, E. G. Arginbaeva, A. V. Shestakov, and A. A. Drozdov, "Influence of the solidification temperature–time parameters on the structure and mechanical properties of nickel aluminide-based alloys," Russ. Metall. (Metally), No. 11, 916–922 (2015).
36. O. A. Bazyleva, A. Bondarenko, O. B. Timofeeva, and A. N. Afanas'ev-Khodykin, "Effect of annealing and high-temperature heating in soldering on the structure and mechanical properties of a nickel aluminide–based alloy," Materialoved., No. 3, 15–20 (2014).
37. Li Ping, Li Shu-Suo, and Han Ya-Fang, "Influence of solution heat treatment on microstructure and stress rupture properties of a $Ni_{3A}l$ base single crystal superalloy IC6SX," Intermetallics **19**, 182–186 (2011).
38. B. A. Grinberg and M. A. Ivanov, *$Ni_3Al$ and TiAl Intermetallics: Microstructure and Deformation Behavior* (IFM URO RAS, Yekaterinburg, 2002).

*Translated by K. Shakhlevich*